Photodissociation Mechanism of Nitramide: A CAS-SCF and MS-CASPT2 Study

Juan F. Arenas, Juan C. Otero, Daniel Peláez, and Juan Soto*

Department of Physical Chemistry, Faculty of Sciences, University of Málaga, E-29071-Málaga, Spain

Received: March 23, 2005; In Final Form: May 24, 2005

The complete active space self-consistent field (CAS-SCF) method combined with the multistate second-order perturbation theory (MS-CASPT2) are used to study the low-lying, singlet and triplet, potential energy surfaces of nitramide. Vertical transition calculations have allowed us to reinterpret the gas-phase UV spectrum of nitramide as the overlapping of two intense bands calculated at 6.46 and 6.52 eV, respectively. The states of relevance in its photochemistry after excitation at different wavelengths have been determined to be up to S_4. From that point on, the most probable dissociation mechanism is determined by considering relative energies among the different stationary points and the major role played by conical intersections connecting S_3/S_2, S_2/S_1, and S_1/S_0 electronic states. The most likely dissociation products are $NH_2(1^2B_1)$, $NO_2(1^2A_1)$, $NO_2(1^2A_2)$, $NO_2(1^2B_2)$, $NO_2(1^2A_1)^*$, $NH_2NO(1^1A'')$, $NO(X^2\Pi)$, and $O(^1D)$. With regards to the influence of triplet states in the photodecomposition of nitramide, our calculations indicate that T_1/S_0 crossing is probable only after radiationless deactivation.

1. Introduction

Nitramide (NH_2NO_2) is the simplest member of the nitramine family, i.e., the simplest closed-shell neutral molecule containing an $N-NO_2$ bond. In addition to its environmental importance as intermediate in the nitrogen oxides elimination, nitramide constitutes a suitable model for the study of the decomposition mechanisms of more complex energetic materials such as RDX (hexahydro-1,3,5-trinitro-s-triazine) or HMX (1,3,5,7-tetranitro-1,3,5,7-tetraazacyclooctane). However, due to its pronounced unstability, its characterization as well as the study of its chemical behavior is rather difficult. For this reason, a theoretical treatment can shed some light on the dissociation dynamics of this compound.

The UV absorption spectrum of nitramide has been obtained in the crystal,[1] in the solution,[2,3a] and in the gas phase.[3b] The gas-phase spectrum exhibits a moderate band centered around 6.3 eV. Additionally, the solution spectrum presents two weak shoulders under 5.0 eV.[2] The theoretical assignment has been accomplished by several authors[1−4] by using different theoretical approaches. Both Stals et al.[2] and Nagakura[3a] studies conclude that the moderate band results in the overlap of two bands, but they differ on their character; while Nagakura interprets this band as an intra NO_2 ($\pi \rightarrow \pi^*$) transition and a charge transfer between a donor (NH_2) and an acceptor (NO_2), Stals et al. reported that $\pi \rightarrow \sigma^*$ and $\pi \rightarrow \pi^*$ transitions were responsible for such a band. On the other hand, Harris[4] shows the moderate band as the result of a $\pi \rightarrow \pi^*$ transition.

To our knowledge, experimental studies on nitramide decomposition, either thermal or photochemical, are still unpublished. Therefore, we will contrast our theoretical results with those of a close structurally related system such as *N*,*N*-dimethylnitramine (DMNA), which is expected to exhibit the main features of nitramide reactivity. Obviously, the methyl fragments will allow chemical pathways which are unreachable for nitramide.

* Corresponding author phone: 34 952132020; fax: 34 9521321047; e-mail: soto@umn.es.

Ground-state DMNA decomposition has been studied by thermal pyrolysis,[5] pulsed laser pyrolysis,[6,7] and IRMPD (Infrared Multiphoton Decomposition) experiments.[8] These studies show that $N-NO_2$ scission is likely to be the main step in DMNA decomposition, although studies carried out by Golden and co-workers[6] have concluded that nitro-nitrite isomerization competes with $N-NO_2$ bond cleavage.

With respect to the UV photolysis of DMNA, Mialocq and Stephenson[9] demonstrated that the photodecomposition at 266 nm yielded $(CH_3)_2N$, $NO_2(X^2A_1)$, and $NO_2(A^2B_2)$ in a monophotonic and collisionless process which took place in less than 6 ps. After excitation of DMNA at 248 nm, McQuaid et al.[10] found as reaction products $OH(A^2\Sigma^+)$, $OH(X^2\Pi)$, $NO_2(A^2B_2)$, $NO_2(X^2A_1)$, and $NO(X^2\Pi)$. Where $NO_2(A^2B_2)$, $NO_2(X^2A_1)$, and $OH(X^2\Pi)$ were generated via monophotonic unimolecular pathways.

Previous computational works on nitramide have been only concerned with decomposition on the ground state. Morokuma and co-workers[11] have studied the ground-state potential energy surface of the $NH_2 + NO_2$ system at different levels of theory. They concluded that the barrierless association of these two radicals leads to formation of NH_2NO_2 and NH_2ONO [eqs 1 and 2].

$$NH_2 + NO_2 \rightarrow NH_2NO_2 \quad (1)$$

$$NH_2 + NO_2 \rightarrow NH_2ONO \quad (2)$$

Subsequent decompositions of these reaction intermediates lead to formation of H_2O, N_2O, H_2NO, and NO.

In the present study, we have investigated the low-lying singlet and triplet potential energy surfaces of nitramide related to its photochemical decomposition after excitation at different wavelengths. Critical points on these surfaces have been located and characterized. The local topology of the potential energy surfaces and the energetic differences among the critical points have allowed us to establish the most likely reaction mechanisms.

10.1021/jp058100k CCC: $30.25
Published on Web 07/26/2005

CHART 1: Orbitals of the Active Space

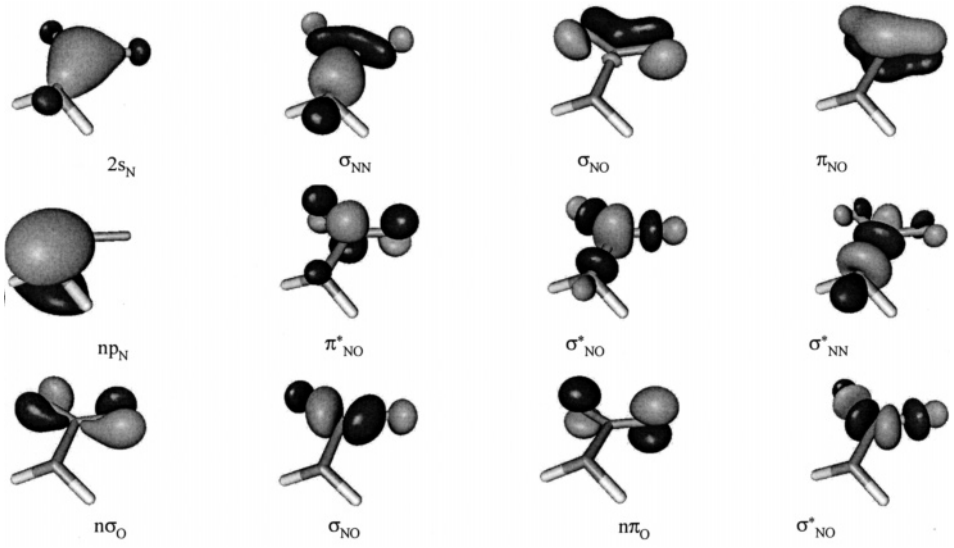

2. Computational Details

Generally contracted basis sets of atomic natural orbital (ANO) type obtained from N,O(14*s*9*p*4d3f)/H(8*s*4*p*3*d*) primitive sets,[12] the so-called ANO-L basis sets, with the N,O[4*s*3*p*2*d*1*f*]/H[3*s*2*p*1*d*] contraction schemes, were used in all of the geometry optimizations of the stationary structures (minima and saddle points) involved in the photolysis of nitramide, which were performed at the complete active space self-consistent field (CAS-SCF)[13] level of theory as implemented in the MOLCAS 6.0 program.[14] The localization of the crossing points (conical intersections and intersystem crossings) were done with the GAUSSIAN program.[15]

The electronic configuration of the ground state is given by

$$(1a'')^2, (1a')^2, (2a')^2, (3a')^2, (4a')^2, (2a'')^2, (5a')^2, (6a')^2, (7a')^2, (3a'')^2, (8a')^2, (4a'')^2, (9a')^2, (5a'')^2, (10a')^2, (6a'')^2$$

which corresponds to the following assignment of the molecular orbitals

$$1s_O, 1s_O, 1s_N, 1s_N, 2s_O, 2s_O, \sigma_{NH2}, 2s_N, \sigma_{NO2}, \sigma_{NH2}, \pi_{NO2}, \sigma_{NO2}, np_N, n\sigma_O, \sigma_{NN}, n\pi_O$$

The choice of the active space has been done according to the criteria used in our previous works on nitromethane.[16] Thus, we have performed CAS-SCF calculations by distributing 16 electrons in 12 orbitals, that is, all valence orbitals have been included except the $2s_O$ and σ_{NH2} ones (Chart 1).

The energies of all critical points have been recomputed with the multistate extension of the multiconfigurational second-order perturbation theory (MS-CASPT2).[17] The CAS-SCF wave functions were used as reference functions in the second-order perturbation treatment, keeping frozen the core orbitals of nitrogen and oxygen as determined in the CAS-SCF calculation. To minimize the contamination of the perturbated wave function by intruder states, the technique of imaginary level shift[18] has been introduced when necessary.

The stationary points were characterized by their CAS-SCF analytic harmonic vibrational frequencies computed by diagonalizing the mass-weighted Cartesian force constant matrix, i.e., the Hessian matrix, ***H***. To perform the vibrational analysis of nonstationary points, such as vertical excitations, the eigenvectors corresponding to rotations, translations, and gradient were projected out of the Hessian matrix as described in a previous article.[19]

Transition dipole moments were computed according to the CAS state interaction (CAS-SI) procedure[20] in conjunction with the perturbatively modified CAS (PMCAS-CI) reference functions obtained as linear combinations of all the states involved in the MS-CASPT2 calculation.

The spin−orbit coupling constants, which are the matrix elements that represent the coupling between two states of different multiplicity,

$$\langle \mathbf{H}_{SO} \rangle_{I,J,r} = \langle {}^1\Psi(M_S)|H_{SO}|{}^J\Psi(M_{S'})\rangle_r, \quad r = x, y, z \qquad (3)$$

have been computed by using an effective one-electron Fock-type spin−orbit Hamiltonian[21] and with the RASSI program implemented in MOLCAS 6.0 ($^l\Psi M_S$ is the wave function including the spin state, and M_S is the component of one sublevel). To avoid the calculation of multicenter one- and two-electron integrals, the atomic mean field integrals (AMFI) have been used.[22] The eigenvectors of the effective Hamiltonian of spin−orbit coupling form a Hermitian matrix. Since the basis set is real and the spin−orbit coupling operator is complex, all spin−orbit coupling constants are off-diagonal. The diagonal elements are the CI energies without spin−orbit couplings. Diagonalizing this Hermitian matrix yields spin−orbit coupled states.[23] To estimate the spin−orbit coupling interaction between two states of different multiplicity, we have used eq 5[24]

$$\mathrm{SOC} = \left(\sum_{Ms} \mathrm{Re}^2\langle \hat{H}_{SO}\rangle_{I,J,Ms} + \mathrm{Im}^2\langle \hat{H}_{SO}\rangle_{I,J,Ms}\right)^{1/2} \qquad (4)$$

Finally, to study the effect of the solvent in the electronic absorption of nitramide, the polarizable continuum model (PCM),[25,26] as implemented in MOLCAS 6.0, has been applied.

3. Results and Discussion

A. Vertical Electronic Excitations. As mentioned in the Introduction section, literature on UV absorption of unconjugated nitramines is scarce and does not provide a unified assignment of the gas-phase UV spectrum of nitramide[2−4] which exhibits a moderate band centered around 6.3 eV, and, in addition to this, two weak shoulders of lower energy appear in solution.[2] Furthermore, it has been shown that the strong band shows a red shifting in higher dielectric solvents.[2]

TABLE 1: MS-CASPT2 Energies of the Vertical Transitions of Nitramide

state	configuration	ΔE^a	ZPE[b]	f [c]
$1^1A'$	G.S.		0.12	
$1^1A''$	$n\sigma_O \rightarrow \pi^*_{NO}$	4.50	0.11	$0.1734 \cdot 10^{-5}$
$2^1A'$	$\sigma_{NN} \rightarrow \pi^*_{NO}$	5.11	0.10	$0.4911 \cdot 10^{-2}$
$2^1A''$	$n\pi_O \rightarrow \pi^*_{NO}$	6.46	0.09	0.1851
$3^1A'$	$np_N \rightarrow \pi^*_{NO}$	6.52		0.1087
$1^3A''$	$n\sigma_O \rightarrow \pi^*_{NO}$	4.29		
$2^3A''$	$n\pi_O \rightarrow \pi^*_{NO}$	4.32		
$1^3A'$	$\sigma_{NN} \rightarrow \pi^*_{NO}$	4.94		

[a] Energy difference in eV. [b] Zero point energy correction in eV. [c] Oscillator strength in a.u.

The vertical excitation energies (singlets and triplets) of nitramide calculated at the MS-CASPT2 level are collected in Table 1 along with the oscillator strength for each transition. From these values we interpret the gas-phase UV absorption spectrum of nitramide as the result of the overlap of two bands of moderate intensity, centered at 6.46 and 6.52 eV, respectively, and the weak shoulders appearing in the solution spectrum as due to the transitions localized at 5.11 and 4.50 eV, respectively.

To study the red shifting in the electronic spectrum, we have performed polarizable continuum model (PCM) calculations for three different solvents, in increasing order of the value of the dielectric constant: namely benzene, methanol, and water. Results are collected in Table 2. From these data the observed shift of the most intense electronic band can be understand as the combined effect of three factors, a pronounced bathochromic shift on the $np_N \rightarrow \pi^*_{NO}$ transition at increasing polarity of the solvent (from 6.52 eV in gas phase to 5.84 eV in water), together with a decrease in its intensity and a slight increase in the intensity of the $n\pi_O \rightarrow \pi^*_{NO}$ and $\sigma_{NN} \rightarrow \pi^*_{NO}$ bands.

B. Singlet Surfaces. The minimum of the ground-state potential energy surface of nitramide corresponds to a nonplanar C_s arrangement[27] (Figure 1a). Above the ground-state surface, three excited stationary states have been localized: (i) a first-order saddle point on the $S_1(1^1A'')$ surface (Sd1, Figure 1b); (ii) a minimum on the $S_2(2^1A')$ surface (Figure 1c); and (iii) a first-order saddle point on the $S_3(2^1A'')$ surface (Sd2, Figure

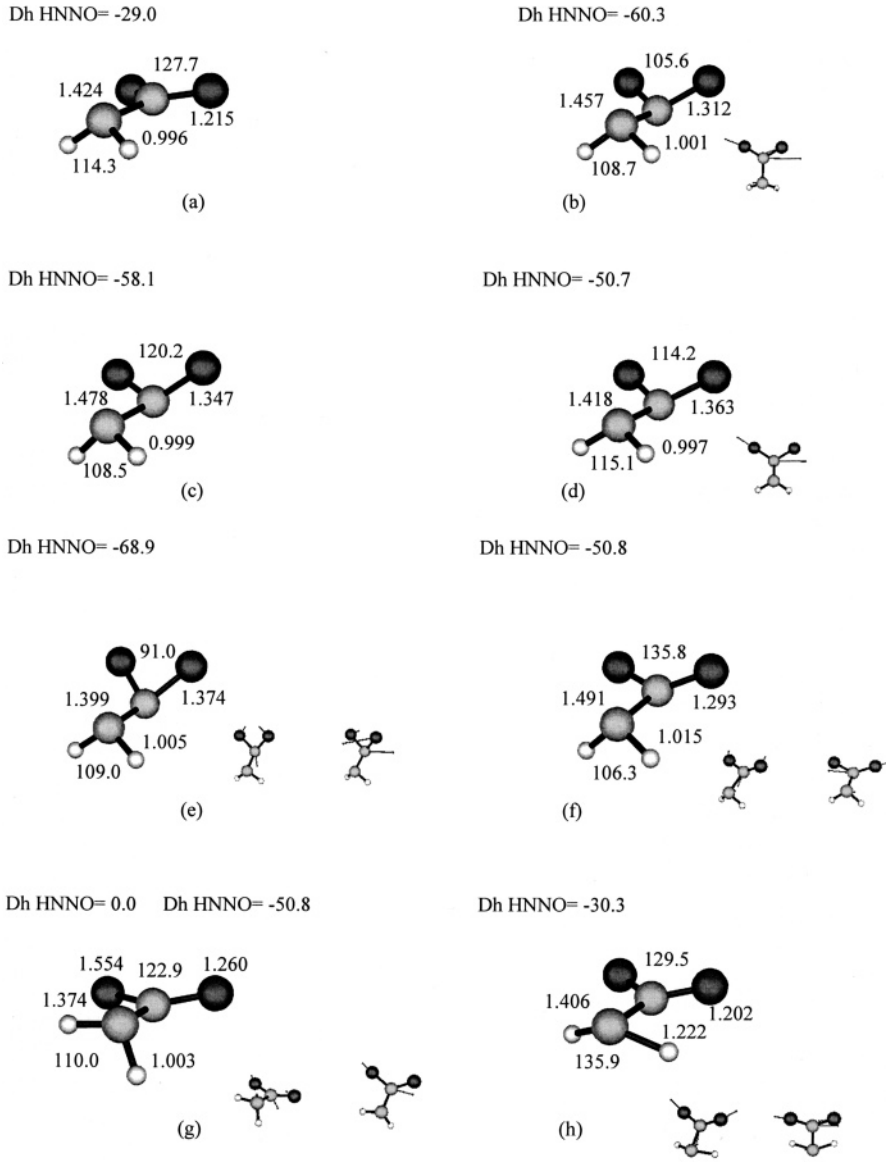

Figure 1. Critical points of nitramide on singlet surfaces. The arrows in the lower structures, (b) and (d), correspond to the imaginary modes. (a) S_0, $1^1A'$ minimum; (b) S_1, $1^1A''$ first-order saddle point; (c) S_2, $2^1A''$ minimum; (d) S_3, $2^1A''$ first-order saddle point; (e) Ci1 S_1/S_0 conical intersection; (f) Ci2 S_2/S_1 conical intersection; (g) Ci3 S_3/S_2 conical intersection; (h) Ci4 S_4/S_3 conical intersection. Under each conical intersection structure, the gradient difference and nonadiabatic coupling vectors are represented.

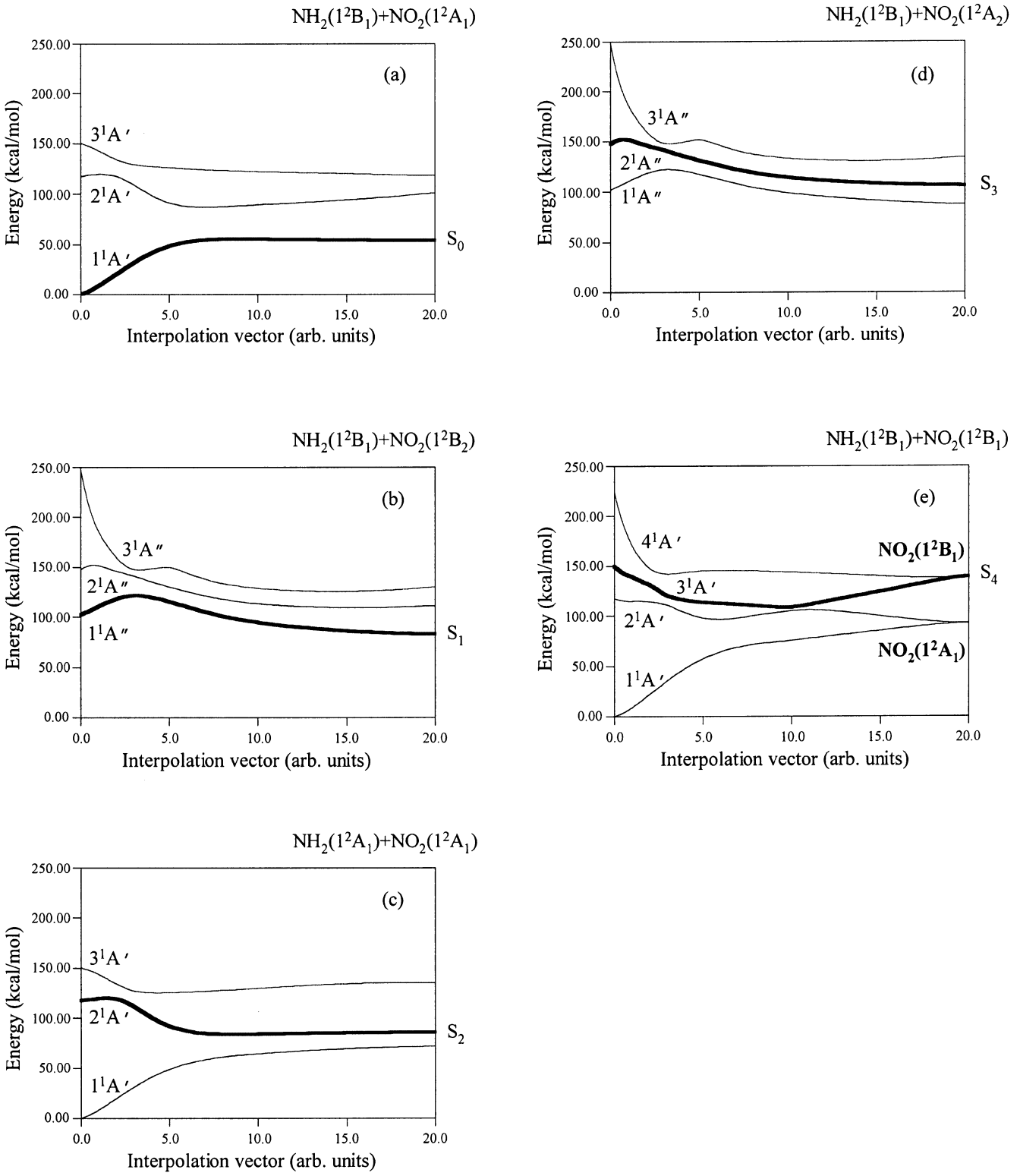

Figure 2. MS-CASPT2 potential energy curves of the low-lying singlet states of nitramide involved in its photodissociation into NH_2 and NO_2. In all of them, initial geometry corresponds to the ground-state minimum and final geometries are indicated on top of the ending axis. All diagrams show states of the same symmetry, (a), (c), and (e) of A′ symmetry, while (b) and (d) of A″. The highlighted line indicates the adiabatic curve of interest. In figure (e) bold inset text represents the electronic state of the NO_2 fragment at the dissociation limit.

1d). The energetics of all the critical points found in this work along with the energies of the products of the respective dissociation processes are collected in Table 3. In addition to the cited stationary points, four conical intersections between singlet surfaces have been found: (i) Ci1 S_1/S_0 (Figure 1e); (ii) Ci2 S_2/S_1 (Figure 1f); (iii) Ci3 S_3/S_2 (Figure 1g); and (iv) Ci4 S_4/S_3 (Figure 1h). The geometries of these conical intersections have been localized with the algorithm implemented in the GAUSSIAN program, i.e., the gradient difference and nonadiabatic coupling vectors are computed using state average orbitals in the manner suggested by Yarkony.[28] This procedure requires the computation of the Hessian at each iteration; however, the contributions that arise from the derivatives of the orbital rotations have been neglected.

TABLE 2: Calculated MS-CASPT2 Energies of the Vertical Transitions and Oscillator Strengths for the Low-Lying Singlet States of Nitramide in Different Solvents

		gas		benzene		methanol		water	
state	configuration	ΔE^a	f^b	ΔE^a	f^b	ΔE^a	f^b	ΔE^a	f^b
$1^1A''$	$n\sigma_O \rightarrow \pi^*_{NO}$	4.50	$0.1734 \cdot 10^{-5}$	4.40	$0.4214 \cdot 10^{-5}$	4.53	$0.2217 \cdot 10^{-5}$	4.54	$0.2040 \cdot 10^{-5}$
$2^1A'$	$\sigma_{NN} \rightarrow \pi^*_{NO}$	5.11	$0.4911 \cdot 10^{-2}$	5.13	$0.7093 \cdot 10^{-2}$	5.13	$0.2242 \cdot 10^{-1}$	5.13	$0.2242 \cdot 10^{-1}$
$2^1A''$	$n\pi_O \rightarrow \pi^*_{NO}$	6.46	0.1851	6.35	0.1976	6.40	0.2025	6.40	0.2026
$3^1A'$	$np_N \rightarrow \pi^*_{NO}$	6.52	0.1087	6.17	0.1093	5.85	$0.9795 \cdot 10^{-1}$	5.84	$0.9675 \cdot 10^{-1}$

[a] Vertical transition energy in eV. [b] Oscillator strength.

TABLE 3: MS-CASPT2 Energies of the Critical Points on the Low-Lying Potential Energy Surfaces of Nitramide

geometry[a]	configuration	weight[b]	energy[c]	ZPE[d]	ΔE^e
m, $1^1A'$	G.S.	90	−260.645 72	0.12	
Sd1, $1^1A''$	$n\sigma_O \rightarrow \pi^*_{NO}$	83	−260.528 72	0.10	3.18
m, $2^1A'$	$\sigma_{NN} \rightarrow \pi^*_{NO}$	68	−260.489 57	0.10	4.25
	$(n\sigma_O)(n\pi_O) \rightarrow (\pi^*_{NO})^2$	16			
Sd2, $2^1A''$	$n\pi_O \rightarrow \pi^*_{NO}$	78	−260.464 51	0.09	4.93
Sd3, $1^3A'$	$\sigma_{NN} \rightarrow \pi^*_{NO}$	84	−260.487 58	0.10	4.30
m, $1^3A''$	$n\pi_O \rightarrow \pi^*_{NO}$	90	−260.532 63	0.10	3.08
Sd4, $2^3A''$	$n\sigma_O \rightarrow \pi^*_{NO}$	86	−260.519 62	0.10	3.43
Ci1, S_1/S_0	$n\sigma_O \rightarrow \pi^*_{NO}$	82	−260.523 76		3.32
Ci2, S_2/S_1	$\sigma_{NN} \rightarrow \pi^*_{NO}$	81	−260.486 25		4.34
Ci3, S_3/S_2	$n\sigma_O \rightarrow \pi^*_{NO}$	84	−260.453 51		5.23
Ci4, S_4/S_3	$np_N \rightarrow \pi^*_{NO}$	85	−260.400 50		6.67
Isc1, T_1/S_0	$n\pi_O \rightarrow \pi^*_{NO}$	87	−260.528 85		3.18
Isc2, T_2/S_1	$(n\sigma_O)(n\pi_O) \rightarrow (\pi^*_{NO})^2$	60	−260.463 98		4.95
Isc3, T_3/S_2	$\sigma_{NN} \rightarrow \pi^*_{NO}$	74	−260.435 54		5.72
dis, $1^1A'$	$NH_2(1^2B_1) + NO(1^2A_1)$	88	−260.559 08		2.36 [f]
dis, $1^1A''$	$NH_2(1^2B_1) + NO(1^2B_2)$	84	−260.512 72		3.62 [f]
dis, $2^1A'$	$NH_2(1^2A_1) + NO(1^2A_1)$	78	−260.508 34		3.74 [f]
dis, $2^1A''$	$NH_2(1^2B_1) + NO(1^2A_2)$	87	−260.475 78		4.62 [f]
dis, $3^1A'$	$NH_2(1^2A_1) + NO(1^2B_1)$	89	−260.448 44		5.37 [f]
dis2[g], $2^1A'$	$NH_2NO(1^1A'') + O(^3P)$	82	−260.446 68		5.42 [f]
dis2[g], $2^1A''$	$NH_2NO(1^1A') + O(^1D)$	83	−260.428 10		5.92 [f]

[a] m, minimum; SdN, nth saddle point; dis, $NH_2 + NO_2$ dissociation limit; dis2, $NH_2NO + O$ dissociation limit. [b] Weight of the configuration in %. [c] Unless indicated, absolute MS-CASPT2 energies in hartrees with a state average CASSCF reference wave function of three states. [d] Zero-point energy correction in kcal/mol. [e] Energy difference in eV. [f] Estimated binding energies in eV referred to ground-state minimum. [g] Although NH_2NO corresponds to the C_1 point group, electronic assignment has been performed following nitramide symmetry criterium.

Once the relevant electronic states in the photodecomposition of nitramide at different wavelengths have been determined, the potential energy curves leading to adiabatic dissociation of the molecule in each valence singlet (and triplet) state have been computed at the MS-CASPT2 level (Figure 2). These curves correspond to the following adiabatic reactions:

$$NH_2NO_2(1^1A') \rightarrow NH_2(1^2B_1) + NO_2(1^2A_1) \quad (5)$$

$$NH_2NO_2(vt, 1^1A'') \rightarrow NH_2(1^2B_1) + NO_2(1^2B_2) \quad (6)$$

$$NH_2NO_2(vt, 2^1A') \rightarrow NH_2(1^2A_1) + NO_2(1^2A_1) \quad (7)$$

$$NH_2NO_2(vt, 2^1A'') \rightarrow NH_2(1^2B_1) + NO_2(1^2A_2) \quad (8)$$

$$NH_2NO_2(vt, 3^1A') \rightarrow NH_2(1^2B_1) + NO_2(1^2B_1) \quad (9)$$

Curves presented in Figure 2 have been built as follows: (i) First, an interpolation vector is calculated by doing the difference between the internal coordinates of the initial and final geometries, that is, S_0 minimum of nitramide and the respective dissociation products. (ii) The distance between the nitrogen atoms of both fragments (NH_2 and NO_2) at the end point of the surface is chosen to be 4.5 Å, yielding a zero charge on both moieties.

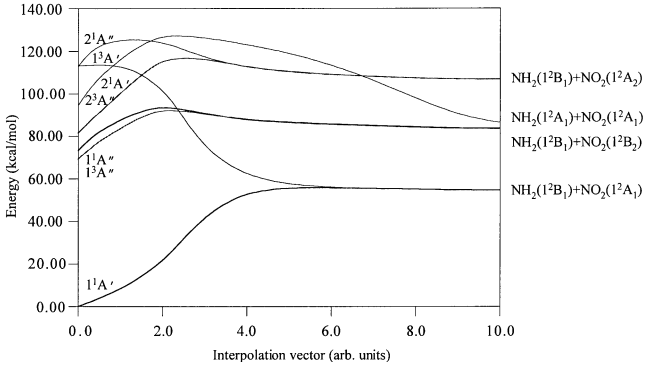

Figure 3. MS-CASPT2 potential energy curves, singlet and triplet, for the dissociation of nitramide starting at the stationary points in each electronic surface. Geometry as well as the electronic state of the dissociated fragments is indicated at the end of each curve. The state ordering is as follows: $1^1A'$, $1^3A''$, $1^1A''$, $2^3A''$, $2^1A'$, $1^3A'$, $2^1A''$.

The following remarks on the above interpolations can be stressed: (i) All of the states, except for S_4, show a direct path going from the Franck−Condon point to dissociation products. (ii) S_1, S_2, and S_3 exhibit barriers for dissociation whose values amount to 21.4, 5.1, and 6.2 kcal/mol, respectively. (iii) The NH_2 fragment is always generated in its electronic ground state, except for the S_2 state.

The same procedure has been followed to compute the energy profiles of the dissociation curves starting at the stationary geometries on each singlet (and triplet) potential energy surface (Figure 3). The main features of these curves do not differ much from those of the previous set of curves; however, the energy barriers for dissociation amount now to 21.6, 31.6, and 24.2 kcal/mol, for S_1, S_2, and S_3, respectively. Likewise, a good estimate of the binding energies can be obtained from the difference in the energy values at the dissociation limit and the energy of the corresponding initial stationary structures, see Table 3. With respect to the triplet state potential energy curves for the respective processes, it is shown that they converge at the dissociation limit; additionally, the estimated energy barriers are 24.3, 36.0, and 0.6 kcal/mol for the T_1, T_2, and T_3 states.

Figure 4 represents the MS-CASPT2 energy profiles running from the Franck−Condon geometry to the respective conical intersections which were localized in this work (Ci1, Ci2, Ci3, and Ci4).

On the basis of the results presented in the above paragraphs, we can make an approximate picture of the dissociation dynamics of NH_2NO_2. Typical excitation wavelengths in the UV spectral region occur around 193 nm (6.42 eV). Therefore, irradiation of a sample of nitramide at this wavelength can populate S_4 or S_3 states, and both are very close energetically (Table 1). As it can be seen in Figure 2e, excitation to the S_4 state would lead to the nonadiabatic dissociation products: NH_2-

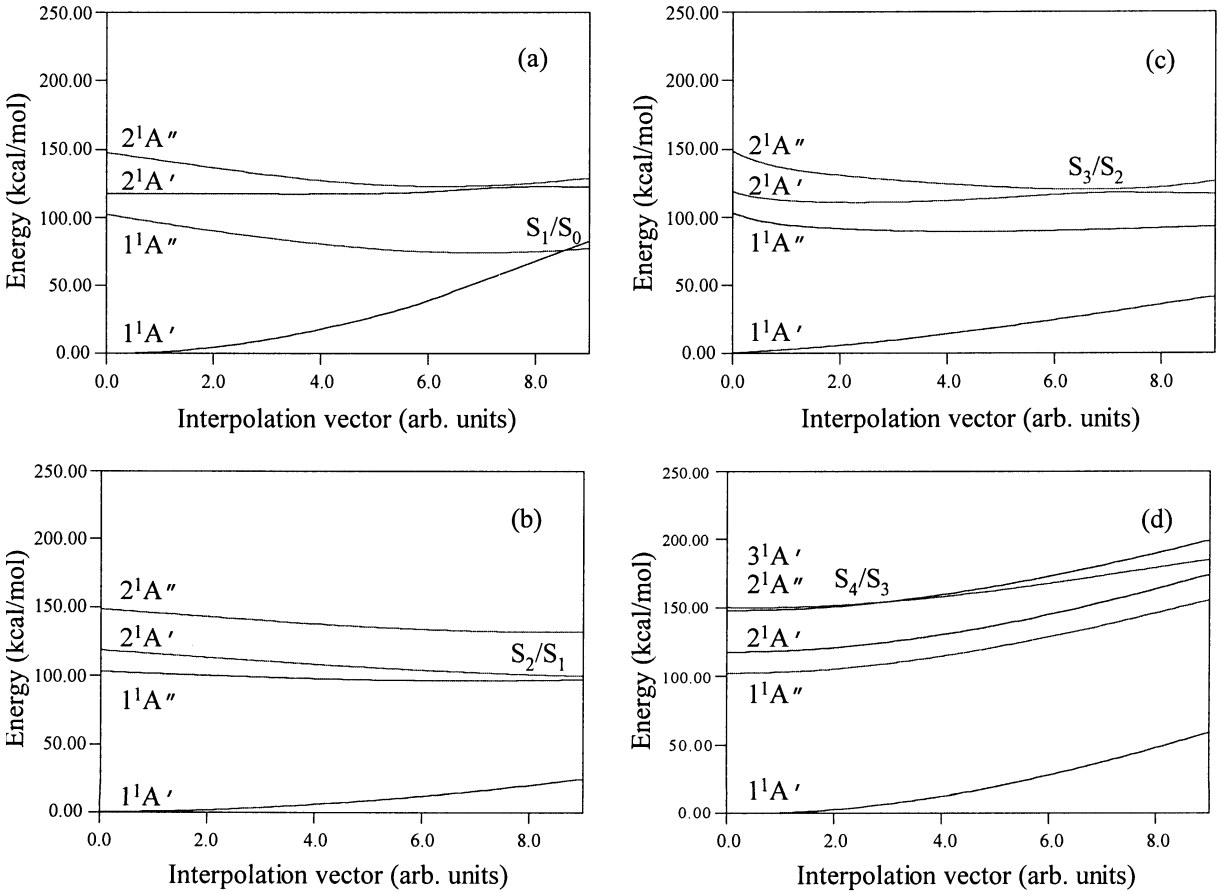

Figure 4. MS-CASPT2 energy profiles for the interpolation vector connecting Franck−Condon geometry and the conical intersections: (a) Ci1, (b) Ci2, (c) Ci3, (d) Ci4. State ordering is as follows: (a), (b), (c) $1^1A'$, $1^1A''$, $2^1A'$, $2^1A''$; (d) $1^1A'$, $1^1A''$, $2^1A'$, $2^1A''$, $3^1A'$.

($^2B_1$) + $NO_2(^2A_1)$. Although there is an S_4/S_3 conical intersection close to the S_4 vertical excitation (Figure 1h), decay through this crossing does not seem very probable because this point is higher in energy than vertical excitation on S_4, and the dissociation path is indeed energetically more favorable.

Excitation starting at the S_3 state gives a completely different picture. The S_3 vertical excitation point has 5 imaginary frequencies, the highest (in absolute value) points to the S_3/S_2 crossing (Ci3, Figure 1g). On the other hand, the only stationary structure localized on the S_3 surface is a first-order saddle point (Sd2, Figure 2d) with its imaginary mode pointing to the S_3/S_2 conical intersection as well. Hence, after excitation on S_3, decay through the S_3/S_2 crossing can be reached via two different routes: (1) direct, $S_3 \rightarrow$ Ci3 and (2) indirect $S_3 \rightarrow$ Sd2 $\rightarrow$ Ci3. The actual path will depend on the specific conditions in which the starting point is prepared. Another possibility is dissociation of the excited nitramide on S_3 to yield $NO_2(1^2A_2)$ plus NH_2 in its ground state.

The plane defined by the nonadiabatic coupling vector and gradient difference vector of Ci3 represented in Figure 1g spans the domain of the potential energy surface leading to oxygen extrusion. So that dissociation into $NH_2NO(1^1A'') + O(^1D)$ after the S_3/S_2 hop is a plausible route. If the previous reaction does not take place, there is a chance for radiationless deactivation to S_2 through the S_2/S_1 conical intersection. Figure 5 represents the MS-CASPT2 energy profile which starts at Ci3 geometry and leads to dissociation into $NH_2NO(1^1A'')$ plus O. The computed barrier for dissociation (12.3 kcal/mol) is, of course, lower than the vertical excitation energy at the starting point of the process. Provided that nitrosamide is generated in an excited

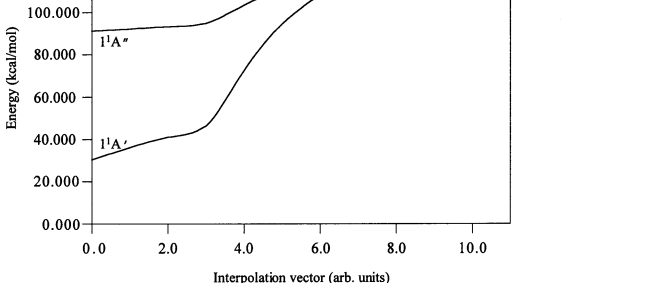

Figure 5. MS-CASPT2 potential energy curves for the dissociation process $NH_2NO(1^1A'') + O(^1D)$, starting at the Ci3 geometry. State ordering is $1^1A'$, $1^1A''$, $2^1A'$, $2^1A''$. Final electronic states are indicated at the end of each curve.

state, it can decompose into $NH_2(1^2B_1)$ and $NO(X^2\Pi)$ in a subsequent step with an exit barrier of 16.4 kcal/mol.

After the S_2/S_1 (Ci2, Figure 1f) jump, the momentum of the molecule is partitioned into the directions of the NAC and GD vectors, that is, the system is directed either to a new surface crossing (Ci1(S_1/S_0), Figure 1e) or it dissociates into $NH_2(1^2B_1)$ + $NO_2(1^2B_2)$ on the S_1 state.

Once the system has reached the S_0 state through Ci1, it has accumulated enough internal energy to dissociate into $NH_2(1^2B_1)$ + $NO_2(1^2A_1)$. It must be pointed out that this 1^2A_1 state could correspond to an excited state and not to the ground state of NO_2; in fact, it is well-known that the A_1 and B_2 states of NO_2 cross along a C_{2v} path.[29] Thus, the preceding discussion implies that nitrogen dioxide can be formed in any of its electronic states

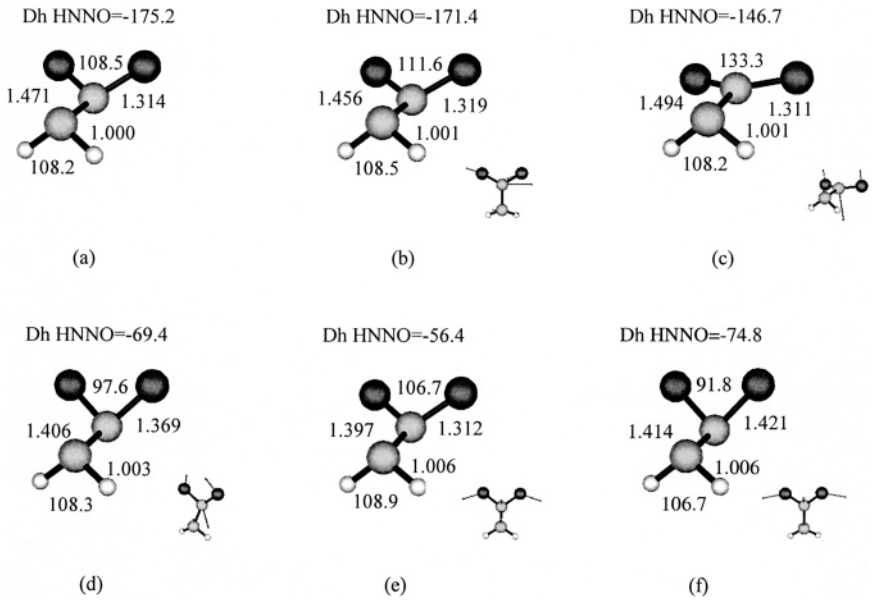

Figure 6. Critical points of nitramide on triplet surfaces. The arrows in the lower structures correspond to the imaginary modes. (a) T_1, $1^3A''$ minimum; (b) T_2, $2^3A''$ first-order saddle point; (c) T_3, $1^3A'$ first-order saddle point; (e) Isc1 T_1/S_0 intersystem crossing; (f) Isc2 T_2/S_1 intersystem crossing; (g) Isc3 T_3/S_2 intersystem crossing. Under each intersystem crossing structure, the gradient difference vector is represented.

1^2A_1, 1^2A_2, 1^2B_2, and $1^2A_1{}^*$, while NH_2 is in all cases generated in its electronic ground state, i.e., 1^2B_1.

C. Triplet Surfaces. Three stationary points have been localized on the triplet surfaces: (i) a minimum on the $T_1(1^3A'')$ surface (Figure 6a); (ii) a first-order saddle point on the T_2-$(2^3A'')$ surface (Sd3, Figure 6b); and (iii) a first-order saddle point on the T_3(Sd4, $1^3A'$) surface (Figure 6c). In addition, we were able to localize three minima (intersystem crossing) in the seam of crossing between singlet and triplet surfaces: (i) Isc1 T_1/S_0 (Figure 6d); (ii) Isc2 T_2/S_1 (Figure 6e); and (iii) Isc3 T_3/S_2 (Figure 6f). The energetics of these critical points are shown in Table 3.

The involvement of intersystem crossings in a photodynamics process is not at all an easy task. To describe intersystem crossing processes quantitatively, one needs not only the potential surfaces involved and spin−orbit couplings as functions of coordinate but also dynamics methods that are capable of describing coupled surfaces where multiple intersections are possible.[30] For example, recently, Schatz and co-workers[30,31] have proposed a methodology to study ISC effects which is based upon a quasiclassical trajectory surface-hopping method to determine dynamical information based on a diabatic representation.

In what follows, we will be content with a qualitative description of the ISC processes involved in the photodissociation dynamics. In principle, the Isc2 and Isc3 crossings can be ruled out because two conical intersections (Ci1 and Ci2) coexist with such intersystem crossings. Hence, it is likely that internal conversion is more efficient than intersystem crossing. A different situation would arise for the $S_0 \rightarrow T_1$ crossing (Isc1, Figure 6d). After decaying to S_0, the crossing region can be sampled increasing the probability P^{ISC} of intersystem crossing. As it is shown in Figure 7, it is clear that the vicinity of Isc1 corresponds to a classical turning point; therefore, nuclear velocity approaches zero, and, moreover, the spin−orbit coupling constant presents a maximum at that point. Consequently, this intersystem crossing is very likely to occur. As the energy difference between ground state minimum geometry and Isc1 is up to 73.3 kcal/mol, it is concluded that, although very probable, Isc1 will only be crossed by energetic molecules coming from excited states after radiationless deactivation. Thus, nitramide can also decompose on the $1^3A'$ state only after internal conversion to S_0; consequently two sources of NO_2-(1^2B_1) are expected, i.e., $S_1(1^1A'')$ and $T_1(1^3A'')$.

4. Summary

The photochemical dissociation mechanisms of nitramide have been studied computationally by means of CAS-SCF/MS-CASPT2 calculations. The relevant electronic states involved in such a process have been determined to be $1^1A'$, $1^1A''$, $2^1A'$, $2^1A''$, and $3^1A'$. Additionally a new assignment of the UV gas-phase spectrum has been proposed; the observed band centered at 6.3 eV, results from the overlapping of two bands, which our calculations predict at 6.46 and 6.52 eV respectively, the latter being mainly responsible for the observed red shifting in higher dielectric solvents. The character of each transition is $n\pi_O \rightarrow \pi^*_{NO}$ and $np_N \rightarrow \pi^*_{NO}$, respectively.

The local topology of the potential energy surfaces at the Franck−Condon region (at the respective stationary points in each surface) has been estimated by means of internal coordinates interpolations between ground-state minimum geometry (stationary geometry) and the optimized geometry of the fragments in the corresponding electronic state. This information together with the relative energy of the critical points provide a very useful tool to elucidate the mechanism of photodecomposition of nitramide. The possible monophotonic products after excitation at 193 nm are $NH_2(1^2B_1)$, $NO_2(1^2A_1)$, $NO_2(1^2A_2)$, $NO_2(1^2B_2)$, $NO_2(1^2A_1)$*, $NH_2NO(1^1A'')$, $O(^1D)$, and $NO(X^2\Pi)$.

Our work can explain the experimental results found in the photodecomposition of dimethylnitramine induced by excitation with 266 and 248 nm wavelengths.[9,10] From the comparison between electronic absorption spectra data and our vertical transition calculations shown in Table 1 it is clear that levels S_1 and S_2 can be populated. Following the previous discussion on the topology and energetics on the Franck−Condon region as well as the profile of the dissociation curves, see Figure 1, it can be established that NO_2 can be only generated in the 1^2A_1 and 1^2B_2 electronic states, in nice agreement with experiment. Moreover, although not described in the literature, our calcula-

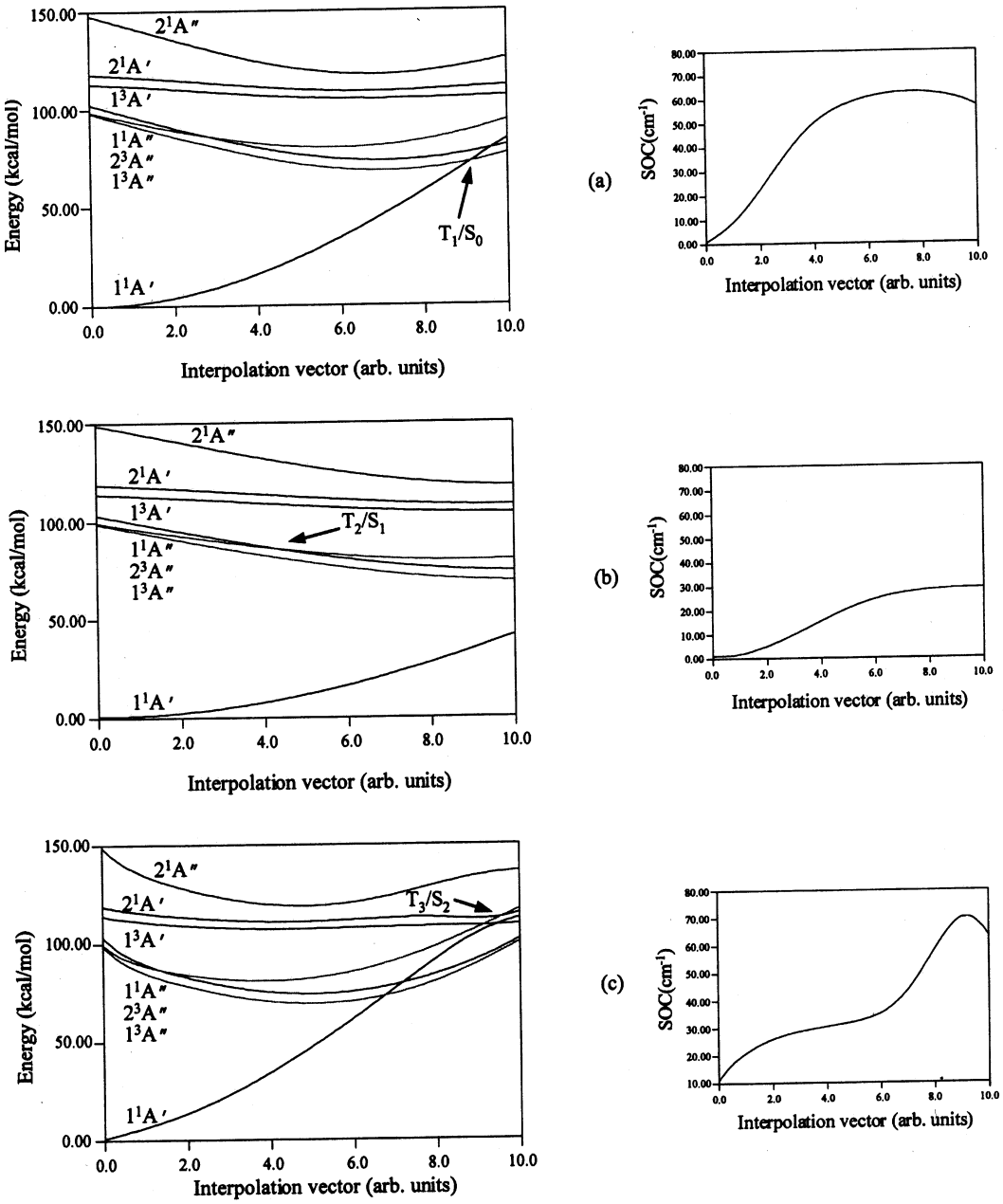

Figure 7. MS-CASPT2 energy profiles of nitramide connecting the Franck−Condon geometry with intersystem crossings: (a) Isc1, T_1/S_0; (b) Isc2 T_2/S_1; (c) Isc3, T_3/S_2. State ordering is as follows: $1^1A'$, $1^3A''$, $2^3A''$, $1^1A''$, $1^3A'$, $2^1A'$, $2^1A''$. Spin−orbit coupling constants for the states of interest are represented on the right-hand.

tions predict that the NH_2 radical can be produced in two different electronic states, $NH_2(1^2B_1)$ and $NH_2(1^2A_1)$, depending on the excitation energy; S_1 yields only $NH_2(1^2B_1)$, while more energetic S_2 excitation may yield both states.

With regard to the influence of triplet states in nitramide photodecomposition, it is shown that after radiationless decay to the ground state, an intersystem crossing process is possible, which would lead to the generation of $NO_2(1^2B_1)$. All the molecular geometries have been represented with the MacMolPlt 5.2.7 program.[32]

Acknowledgment. This research has been supported by the Ministerio de Ciencia y Tecnología (Project BQU2003-01426). D. Peláez thanks the Ministerio de Ciencia y Tecnología for his Research Grant No. BES-2004-6033. The authors thank SCAI (University of Málaga) economical support for providing the MOLCAS 6.0 software package.

References and Notes

(1) Häussler, A.; Klapötke, T.; Piotrowski, H. *Z. Naturforsch.* **2002**, *57b*, 151.

(2) Stals, J.; Barraclough, C. G.; Buchanan, A. S. *Trans. Faraday Soc.* **1969**, *65*, 904.

(3) (a) Nagakura, S. *J. Chem. Phys.* **1955**, *23*, 1441. (b) Kaya, K.; Kuwata, K.; Nagakura, S. *Bull. Chem. Soc. Jpn.* **1964**, *37*, 1055.

(4) Harris, L. E. *J. Chem. Phys.* **1973**, *58*, 5615.

(5) Oxley, J. C.; Hiskey, M.; Naud, D.; Szekeres, R. *J. Phys. Chem.* **1992**, *96*, 2505.

(6) Nigenda, S. E.; McMillen, D. F.; Golden, D. M. *J. Phys. Chem.* **1989**, *93*, 1124.

(7) Stewart, P. H.; Jefreys, J. B.; Zellweger, J.-M.; McMillen, D. F. *J. Phys. Chem.* **1989**, *93*, 3357.

(8) Lazarou, Y. G.; Papagiannakopoulos, P. *J. Phys. Chem.* **1990**, *94*, 7114.

(9) Mialocq, J.-C.; Stephenson, J. C. *Chem. Phys. Lett.* **1986**, *123*, 390.

(10) McQuaid, M. J.; Miziolek, A. W.; Sausa, R. C.; Merrow. C. N. *J. Phys. Chem.* **1991**, *95*, 2713.

(11) Mebel, A. M.; Hsu, C.-C.; Lin, M. C.; Morokuma, K. *J. Chem. Phys.* **1995**, *103*, 5640.

(12) Widmark, P.-O.; Malmqvist, P.-Å.; Roos, B. O. *Theor. Chim. Acta* **1990**, *77*, 291.

(13) Roos, B. O. In *Advances in Chemical Physics; Ab Initio Methods in Quantum Chemistry II*; Lawley, K. P., Ed.; Wiley: Chichester, England, 1987; Chapter 69, p 399.

(14) Andersson, K. et al. MOLCAS Version 6.0, Lund University, Sweden.

(15) Frisch, M. J. et al. Gaussian 03, Revision B.04.

(16) (a) Arenas, J. F.; Centeno, S. P.; López-Tocón, I.; Peláez, D.; Soto, J. *J. Mol. Struct. (THEOCHEM)* **2003**, *630*, 17. (b) Arenas, J. F.; Otero, J. C.; Peláez, D.; Soto, J. *J. Chem. Phys.* **2003**, *119*, 7814. (c) Arenas, J. F.; Otero, J. C.; Peláez, D.; Soto, J.; Serrano-Andrés, L. *J. Chem. Phys.* **2004**, *121*, 4127. (d) Arenas, J. F.; Otero, J. C.; Peláez, D.; Soto, J. *J. Chem. Phys.* **2005**, *122*, 084324.

(17) Finley, J.; Malmqvist, P.-Å.; Roos, B. O.; Serrano-Andrés, L. *Chem. Phys. Lett.* **1998**, *288*, 299.

(18) Forsberg, N.; Malmqvist, P.-Å. *Chem. Phys. Lett.* **1997**, *274*, 196.

(19) Arenas, J. F.; Marcos, J. I.; López-Tócon, I.; Otero, J. C.; Soto, J. *J. Chem. Phys.* **2000**, *113*, 2282.

(20) Malmqvist, P.-Å. *Int. J. Quantum Chem.* **1986**, *30*, 470.

(21) Hess, B. A.; Marian, C.; Wahlgren, U.; Gropen, O. *Chem. Phys. Lett.* **1996**, *251*, 965.

(22) Malmqvist, P.-Å.; Roos, B. O.; Schimmelpfenning, B. *Chem. Phys. Lett.* **2002**, *357*, 230.

(23) Ribbing, C.; Gilliams, B.; Pierloot, K.; Roos, B. O.; Karlström, G. *J. Chem. Phys.* **1998** *109*, 3145.

(24) Furlani, T. R.; King, H. F. *J. Chem. Phys.* **1985**, *82*, 5577.

(25) Barone, V.; Cossi, M. *J. Phys. Chem. A* **1998**, *102*, 1995.

(26) Cossi, M.; Rega, N.; Scalmani, G.; Barone, V. *J. Chem. Phys.* **2001**, *114*, 569.

(27) Tyler, J. K. *J. Mol. Spectrosc.* **1963**, *11*, 39.

(28) Yarkony, D. R. *J. Chem. Phys.* **1990**, 92, 2457.

(29) Davidson, E. R.; Borden, W. T. *J. Phys. Chem.* **1983**, *87*, 4783.

(30) Maiti, B.; Schatz, G. C. *J. Chem. Phys.* **2003**, *119*, 12360.

(31) Hoffmann, M. R.; Schatz, G. C. *J. Chem. Phys.* **2000**, *113*, 9456.

(32) Bode, B. M.; Gordon, M. S. *J. Mol. Graphics Modell.* **1999**, *16*, 133.